Correspondence

A Novel Pulse-Echo Technique for Medical Three-Dimensional Imaging

Ahmed Yamani

***Abstract*—A new pulse-echo imaging technique for close near-field applications is proposed. Based on the theory developed for the continuous-wave automatic focusing technique (CWAFT), it uses instead, a frequency-domain phase compensation through a convolutional mechanism. In addition, the scanned frequencies of the transmitted CW signals are sent simultaneously in a pulse that is used for the data acquisition and processing. The pulse-echo nature of this technique makes it a candidate for further development and evaluation for ultrasonic three-dimensional (3-D) medical imaging and nondestructive testing. Furthermore, the "spike-like" nature of the back propagator in the frequency domain is used to half the data acquired. This alleviates most of the drawbacks of the CWAFT in data acquisition and processing. Simulation results are presented for both two-dimensional (2-D) and 3-D targets.**

***Index Terms*— Automatic focusing, angular spectrum decomposition, depth of focus, multifrequency reconstruction, pulse-echo imaging.**

I. Introduction

Ultrasonic imaging for medical diagnostic application is a well-established technique in clinical practice today. A variety of equipment is based on electronically scanned phased-array transducers, which generate linear or sector-format images, displaying soft-tissue structures typically up to 20-cm depth at a rate of 30 frames/s. Focusing is usually implemented electronically by means of delay lines, which are adjusted to compensate the differences in propagation path from the focal point to the array elements.

An important feature of any imaging system concerns its ability to unambiguously resolve the details of a target. In general, resolution and ambiguity can be governed by a suitable choice of the collecting aperture size, its shape, and the effective weighting function applied as the target information is recorded and processed to produce an image. However, for a given set of focusing conditions, these properties can only be maintained over a limited region of image space, which is usually known as the depth of field or depth of focus (DOF) [1]. Beyond this region, image degradation becomes unacceptable. Moreover, medical imaging (MI) systems usually operate in the near field of the recording aperture where the DOF is particularly small and leads to difficulties in image interpretation.

It has been demonstrated in [1] that substantial improvements in image quality can be achieved in the very close near field through the use of time-domain compensation in continuous-wave (CW) imaging systems. The only drawback of this CW automatic focusing technique (CWAFT) is that it requires sophisticated hardware and a considerable amount of data acquisition and processing. Being multifrequency in nature, the three-dimensional (3-D) arrays needed to process the data are much too large for the random access memory (RAM) of any commercial PC. Hence, external disk memory is needed and this can be time consuming, particularly if implemented in real-time imaging systems.

The objective of this contribution is to show that the CWAFT can be extended to the pulse-echo imaging systems while maintaining the automatic focusing capabilities. In addition, considerable improvements in data acquisition and processing is obtained. This is achieved by first, synthesizing a pulse whose frequency content is identical to the scanned frequencies originally used in the CWAFT and second, by applying instead, the phase compensation in the frequency domain through a convolutional mechanism. The pulse-echo nature of this new procedure (called, in this paper, PAFT) makes it suitable for near-field pulse-echo imaging found in nondestructive testing (NDT) and in MI. Furthermore, it will be shown that the "spike like" nature of the correction factor in the frequency domain enables the use of only half the bandwidth required by the CWAFT with no apparent loss in image quality.

Section II-A discusses briefly the theory of the CWAFT and exposes its drawbacks. In Section II-B we propose a new method based on the convolution theorem and show how the scanned frequencies synthesize a pulse that is used to improve the data acquisition and the processing time required to reconstruct high-quality images. The new procedure is validated in Section III using simulated data for both two-dimensional (2-D) and 3-D imaging systems. Section IV presents the conclusion and discusses possible implementations of the proposed technique in MI systems.

II. Theory

A. CW Automatic Focusing Technique

The AFT theory will be briefly presented in this section, and the drawback in data acquisition and processing inherent in the AFT algorithm will be outlined. It is assumed throughout this paper that the data is collected using a series of measurements from a "point-like" sensor. Such a sensor might consist of an array of omnidirectional transducers or a single transducer scanned over the received aperture.

The AFT algorithm is based upon a mathematical analysis technique, known as angular spectrum decomposition [2]. Data is recorded over a range of frequencies within the bandwidth of a typical transducer, and the method can be applied in circumstances where the target lies in the very close near field of the recording aperture.

With reference to Fig. 1, let $U(x, y, 0; f)$ represent the complex (real and imaginary) ultrasonic pressure field measured over a 2-D aperture located at $z = 0$, where the frequency f is scanned over the transducer bandwidth Δf. By 2-D Fourier transform, with respect to the spatial coordinates x and y, this pressure field can be represented by its angular spectrum

$$A(s_x, s_y, 0; f) = \int_{-\infty}^{\infty}\int_{-\infty}^{\infty} U(x, y, 0; f) \cdot \exp[-i2\pi(xs_x + ys_y)]\, dx\, dy \tag{1}$$

where $i = \sqrt{-1}$, s_x and s_y are the spatial frequencies. The angular spectrum of a complex pressure field measured at the plane $z = 0$ is related in [2] to that at any other plane z as

$$A(s_x, s_y, 0; f) = A(s_x, s_y, z; f)B(s_x, s_y, z; f) \tag{2}$$

Manuscript received August 8, 1996; revised April 29, 1997. The Associate Editor responsible for coordinating the review of this paper and recommending its publication was M. W. Vannier.

The author is with King Fahd University of Petroleum, P.O. Box 1811, Dhahran 31261 Saudi Arabia (e-mail: myamani@dpc.kfupm.edu.sa).

Publisher Item Identifier S 0278-0062(97)09300-2.

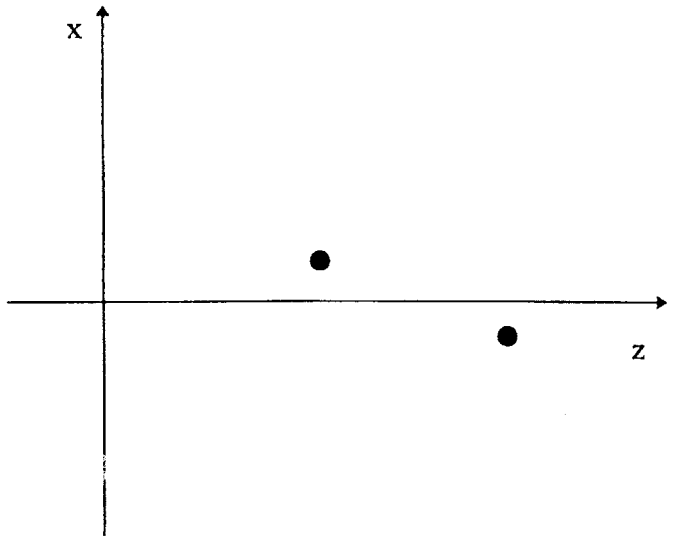

Fig. 1. Imaging configuration used.

where

$$B(s_x, s_y, z; f) = \exp\left(i2\pi \frac{nfz}{v}\sqrt{1 - \left(\frac{s_x v}{nf}\right)^2 - \left(\frac{s_y v}{nf}\right)^2}\right) \tag{3}$$

is known as the propagator filter, v is the phase velocity of the wave, and n is an integer equal to one for a fixed transmitter-scanned receiver and equal to two for a simultaneously scanned transmitter/receiver [3]. If a target is located a distance z from the transmit-receive aperture, then (2) represents the basis of a multifrequency backward wave propagation imaging scheme. The angular spectrum of the received complex acoustic pressure field can be back propagated to the target plane by multiplying (2) by the back propagator filter $B^{-1}(s_x, s_y, z; f)$ to yield an in-focus target image in the spatial image domain. It is interesting to note that Busse [3] viewed (2) as a series of images, in the spatial frequency domain, at different frequencies. By averaging these images over all the frequencies considered, followed by the application of a 2-D inverse Fourier transformation with respect to the spatial coordinates, he obtained high-quality images as compared to the single-frequency reconstruction algorithm traditionally used in CW imaging systems. However, this elegant approach, not only requires a prior target range information z, but it fails to produce in-focus images of a 3-D target whose dimension in the z-direction exceeds the DOF. In addition, undesirable distortions inherent in the backward wave propagation algorithm [1] can further complicate any diagnostic process. This problem has been solved by the CWAFT [1] as follows.

Instead of back propagating (2) using the filter $B^{-1}(s_x, s_y, z; f)$, an inverse Fourier transform with respect to f is used to yield the time-domain angular spectrum $A(s_x, s_y, 0, t)$. A new back propagator is derived in [1] to compensate simultaneously the time-domain angular spectrum of targets situated at widely different ranges from the transmit-receive aperture. This back propagator is given by

$$B'(s_x, s_y; t) = \exp\left[-i2\pi f_0 t\left[1 - \left(\frac{s_x\lambda_0}{n}\right)^2 - \left(\frac{s_y\lambda_0}{n}\right)^2\right]\right] \tag{4}$$

where f_0 and λ_0 are the frequency and the wavelength, respectively, at the center of the transducer bandwidth. The resultant data is transformed back to the frequency domain via a one-dimensional (1-D) Fourier transform. It is shown that at the center frequency f_0, the nonlinear phase due to the propagator defined by (3) is completely removed from the resultant angular spectrum. Upon application of the 2-D inverse Fourier transform with respect to the spatial frequencies s_x and s_y, an in-focus 3-D image is obtained regardless of the axial dimension of the target(s).

The intensity of a pixel at x, y, obtained from the CWAFT algorithm can, thus, be expressed as

$$I(x,y) = |F^{-1}_{s_x,s_y}\left[F_t\left[F_f^{-1}[F_{x,y}[U(x,y,0;f)]] \times B'(s_x, s_y, t)\right]|_{f=f_0}\right]|^2 \tag{5}$$

where $F^{-1}_{s_x,s_y}[\cdot]$ represents a 2-D inverse Fourier transform with respect to s_x and s_y, while $F_t[\cdot]$ represents a 1-D Fourier transform with respect to t. As can be seen from (5), the CWAFT algorithm relies heavily on both temporal and spatial Fourier transforms. Although, the algorithm can be efficiently implemented using more commonly available computer hardware, such as array processors, accelerator cards, or digital signal processing (DSP) chips, it will be shown that a simplification of (5) yields a new AFT procedure which greatly reduces the acquired data and the number of fast Fourier transforms (FFT's) used.

B. Pulsed Automatic Focusing Technique

First, the PAFT imaging procedure can be developed by transmitting a pulsed signal $p(t)$ say, that is synthesized by the scanned frequencies used in the CWAFT such that the recorded complex waveform $u(x, y, 0; t)$ over the aperture is related to $U(x, y, 0, f)$ by

$$u(x, y, 0; t) = F_f[U(x, y, 0; f)].$$

Knowing that the complex pressure field recorded at the ith array element and due to a point-reflector can be expressed as

$$U(x, y, 0; f) = \text{rect}\left[\frac{f - f_0}{\Delta f}\right]\exp\left(-j\frac{4\pi f R_i}{v}\right)$$

where $\text{rect}[\cdot]$ is the rectangular function, and R_i is the distance between the point-reflector and the ith array element. It is shown in [5] that the envelope of the transmitted pulse $p(t)$ is given by

$$a(t) = \frac{\sin\left(\frac{M\pi R}{R_m}\right)}{\sin\left(\frac{\pi R}{R_m}\right)} = 1 + 2\sum_{n=1}^{(M-1)/2}\cos\left(\frac{2\pi n R}{R_m}\right) \tag{6}$$

where M is the number of frequencies originally scanned in the CWAFT, $R = vt/2$ denotes the variable in the range domain, and R_m is a maximum range related to the frequency sampling interval δf by $R_m = v/2\delta f$.

Second, a close examination of (5) reveals that the product in the inner brackets can be simplified using the convolution theorem [4], i.e.,

$$F_t[A(s_x, s_y, t) \times B'(s_x, s_y, t)]|_{f=f_0} = A(s_x, s_y, f) \otimes B'(s_x, s_y, f)|_{f=f_0} \tag{7}$$

where the time-domain angular spectrum $A(s_x, s_y, t)$ is given by $A(s_x, s_y, t) = F_{x,y}[u(x, y, 0; t)]$, $\otimes$ denotes the convolution operator. $B'(s_x, s_y, f) = F_t[B'(s_x, s_y, t)]$ which can be easily shown to be

$$B'(s_x, s_y, f) = T_m \exp[-i\pi T_m(f - f_s)]\text{sinc}[T_m(f - f_s)] \tag{8}$$

where T_m is the inverse of the frequency sampling interval δf, $\text{sinc}(x) = \sin(\pi x)/\pi x$, and f_s defines the position, along the frequency axis, of the main beam of the sinc function and is given by

$$f_s = f_0\left[1 - \left(\frac{s_x\lambda_0}{n}\right)^2 - \left(\frac{s_y\lambda_0}{n}\right)^2\right]. \tag{9}$$

From (8) and (9), it can be concluded that for a given imaging system, the backpropagator $B'(s_x, s_y, f)$ can be generated and stored beforehand. This enhances the processing time of the PAFT. Furthermore, as (7) describes the convolution at the point $f = f_0$ which is equal to a sum of products, this can be rearranged in a form suitable for vector multiplication as follows:

If the number of frequencies scanned around the center frequency f_0 in the CWAFT is $M = 2N + 1$, then the kth frequency can be written as

$$f_k = f_0 + k \times \delta f, \qquad k \in [-N, N]$$

and the angular spectrum of the acoustic pressure field at this frequency f_k can be written for simplicity as

$$A(s_x, s_y, f_k) = A_{s_x s_y k}$$

which can be put in an angular spectrum vector, in a simplified form, as

$$\overline{A}_{s_x s_y} = (A_N, A_{N-1}, \cdots, A_0, \cdots, A_{-N+1}, A_{-N})^T_{s_x s_y}$$

where T denotes the transpose operation. Similarly, the back propagator filter defined by (8) can be written in a vector form as

$$\overline{B}'_{s_x s_y} = (B'_{-N}, B'_{-N+1}, \cdots, B'_0, \cdots, B'_{N-1}, B'_N)^T_{s_x s_y}.$$

Using (5) and (7), the frequency-compensated angular spectrum can, thus, be written as

$$\begin{aligned} A'(s_x, s_y, f_0) &= A(s_x, s_y, f) \otimes B'(s_x, s_y, f)|_{f=f_0} \\ &= \overline{A}^T_{s_x s_y} \cdot \overline{B}_{s_x s_y}. \end{aligned} \tag{10}$$

Equation (5) is, thus, simplified to

$$I(x, y) = |F^{-1}_{s_x, s_y}\left[\overline{A}^T_{s_x s_y} \cdot \overline{B}_{s_x s_y}\right]|^2. \tag{11}$$

The frequency-compensating PAFT algorithm can be summarized in the following steps.

1) Transmit the pulse $p(t)$ whose envelope is given by (6).
2) At each point of the aperture, Fourier transform the received waveforms $u(x, y, 0; t)$ to get the complex pressure field $U(x, y, 0; f)$.
3) Apply a 2-D FFT, with respect to the spatial coordinates x and y, to get the angular spectrum $A(s_x, s_y, f)$
4) For each spatial frequency s_x and s_y, form the vectors $\overline{A}_{s_x s_y}$, and $\overline{B}_{s_x s_y}$ from the angular spectrum and the back-propagator filter, respectively.
5) Evaluate the vector multiplication as defined by (10).
6) Apply a 2-D inverse FFT on the result, and form the image from the square of the magnitude of the data.

The "spike-like" nature of the back propagator in the frequency domain $B'(s_x, s_y, f)$ can be used to further simplify the PAFT procedure. With reference to (8) and (9), it can be seen that for any given spatial frequencies (s_x, s_y), the position of the back propagator main beam is always below the center frequency f_0. This means that for any frequency f greater than f_0, the amplitude of the back propagator is negligibly small, which reduces the contribution of the lower side band of $A(s_x, s_y, f)$ to the vector product defined by (10). This implies that only the upper side band of the pulsed acoustic pressure field $u(x, y, 0; t)$ and the lower side band of the back propagator are to be used *a priori*, for successful operation of the PAFT. The new procedure hence obtained is referred to as half-bandwidth PAFT.

The contribution of this paper; although it seems simple in its nature; is unique in that it uses a pulsed signal for the data acquisition and processing. This enables the AFT procedure to be extended to the pulse-echo imaging systems as is the case in MI and in NDT. In addition, the automatic focusing is implemented through vector products in the frequency-domain which reduces, considerably, the number of FFT's used.

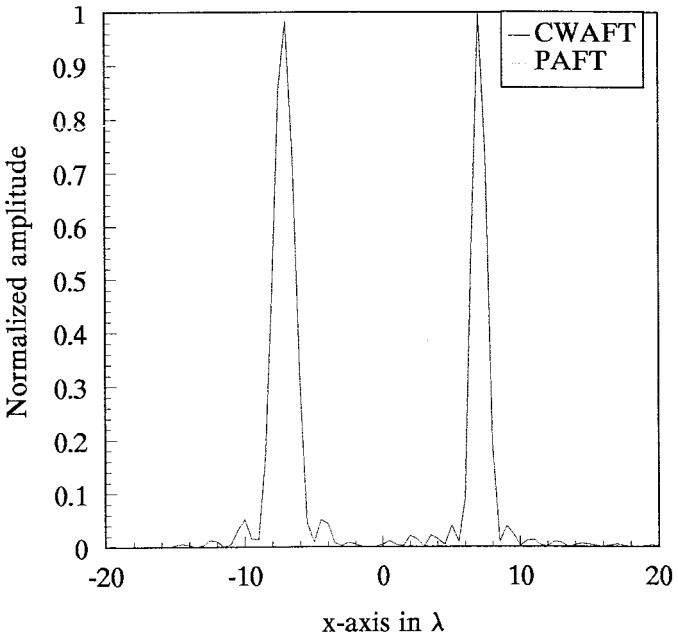

Fig. 2. Image of the two point reflectors of Fig. 1 obtained using CWAFT and PAFT.

III. Simulations

To test the PAFT algorithm as outlined in the previous section, a computer program was written to generate (simulate) the acoustic pressure field that would be observed at the receiving square aperture when a pulse $p(t)$ is transmitted. Fig. 1 shows the configuration of a 1-D imaging system operating in water at a wavelength of $\lambda_0 =$ 8 mm, where the two point-targets are located at $75\lambda_0$ and $112\lambda_0$ from a $37\lambda_0$ transmit-receive aperture sampled at $\lambda_0/2$. Each target is displaced from the central axis by $6.25\lambda_0$. Since the near field of this imaging system extends up to a range of $684.5\lambda_0$, the point-reflectors considered in this paper lie in the close near field of the receiving aperture as is the case in MI. The transmitted pulse is synthesized by $M = 21$ frequencies centered at f_0. This yields a pulse bandwidth $\Delta f = 0.05 f_0$, which is well within that of a typical transducer. First, the equivalence of the CWAFT and the PAFT is tested and it is found that the image obtained from the PAFT procedure is identical to its counterpart image obtained from the CWAFT. The small discrepancies between the resulting images shown in Fig. 2, can be attributed to the extra forward and inverse FFT's required by the CWAFT at each spatial frequency.

The "spike-like" nature of the back-propagator filter in the frequency domain is shown in Fig. 3, where it is clearly shown that the main beam position is always below the center frequency f_0 as demonstrated in the previous section. This phenomenon is used here to further improve the processing time of the PAFT. When the lower side band of the back propagator is used in the compensation process, the reconstructed image is found to be remarkably similar to that obtained from the PAFT. This result is shown in Fig. 4.

The target configuration shown in Fig. 1 is also examined using a 2-D $(37\lambda_0 \times 37\lambda_0)$ transmit-receive aperture with the point-targets located at $75\lambda_0$ and $150\lambda_0$ and displaced from the central axis by $12.5\lambda_0$. When the half-bandwidth PAFT is used, a simultaneous in-

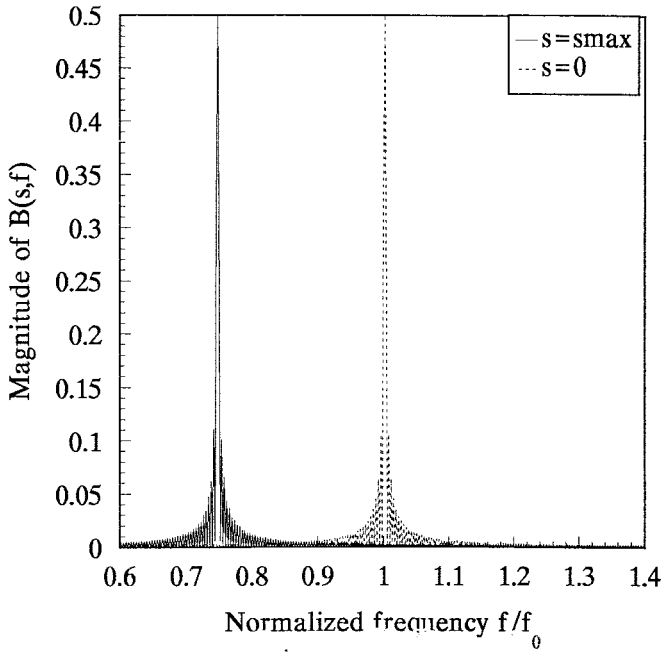

Fig. 3. Frequency response of the back-propagator filter at spatial frequencies $s - s\max$, and $s = 0$.

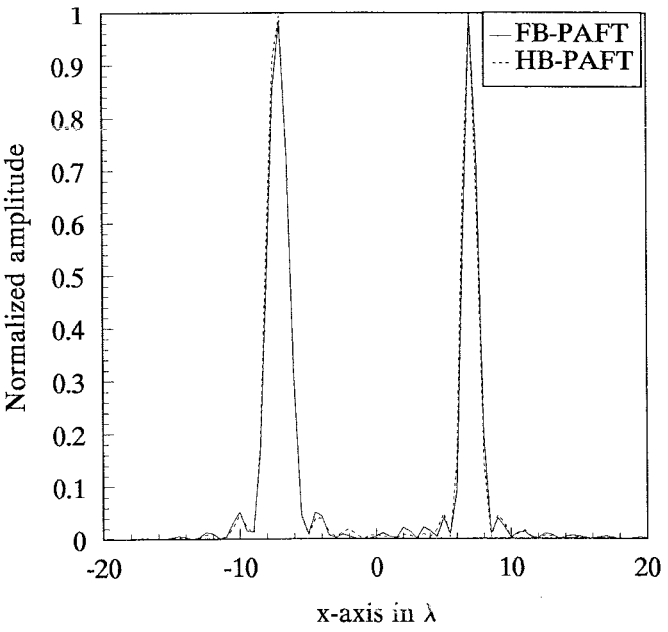

Fig. 4. Image of the two point-reflector of Fig. 1 obtained using FB-AFT and HB-PAFT.

focus image is obtained as shown in Fig. 5, where the $1/r$ space attenuation is included and is clearly shown. Had the CWAFT been used instead, then 2^{2n+1} additional FFT's would have been used, where 2^n is the size of the FFT array considered.

Finally, the case of a 3-D target consisting of eight point reflectors, each located at the corner of a cube of $25\lambda_0$ side, is considered. For this test, the center of the cube is placed on the z-axis at $110\lambda_0$ from a $(37\lambda_0 \times 37\lambda_0)$ transmit-receive aperture, with two faces initially parallel to the aperture. To have a perspective view of this 3-D target, the cube is then rotated by 25° and 15° about the x and y axes, respectively. When the half-bandwidth PAFT is used, a simultaneous in-focus image of the point-reflectors is obtained as shown in Fig. 6.

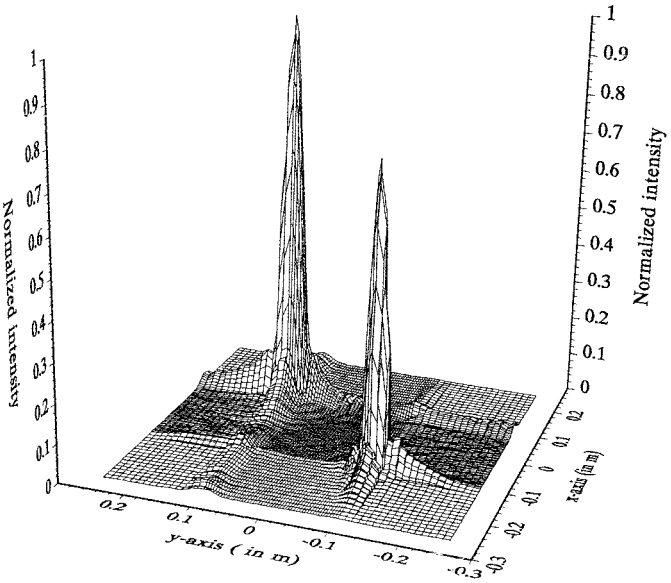

Fig. 5. Three-dimensional image of the targets configuration of Fig. 1 obtained using HB-PAFT.

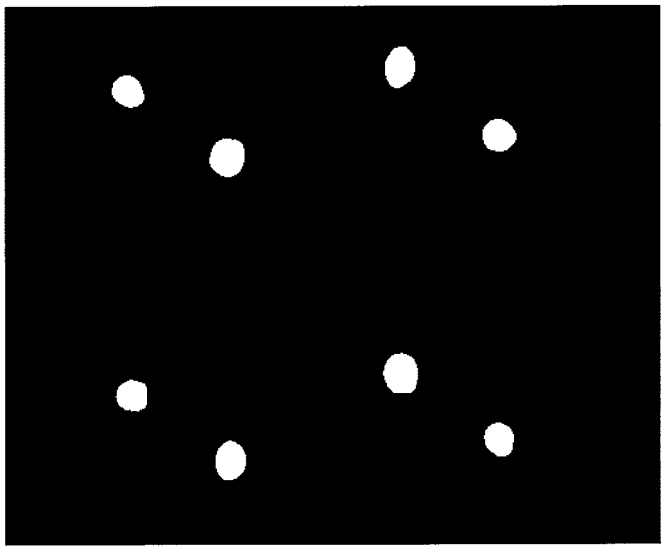

Fig. 6. Half-bandwidth PAFT reconstruction of a cube.

IV. Conclusion

In this paper, a new PAFT is developed for near-field ultrasonic 3-D imaging applications. Based on the theory developed for the CWAFT, it has been shown that the phase compensation can be used, instead, in the frequency domain through a convolutional mechanism which saves a great number of FFT's originally required by the CWAFT algorithm. Furthermore, the back propagator is shown to have a "spike-like" nature in the frequency domain whose main beam position is always less than or equal to f_0. This means that for frequencies such that $f > f_0$, the magnitude of the back propagator is negligibly small and, hence, its contribution to the compensation process defined by (10) can be ignored. Due to the convolutional nature of the compensation process defined by (10), the lower side band of the acoustic pressure is *nulled* by the back propagator upper side band. This implies that the upper side band of the acoustic pressure field $u(x, y, t)$ is to be considered and that only the lower side band of the back propagator can be stored and used, *a priori*, for

successful operation of the PAFT. Simulation results are presented for both 2-D and 3-D targets and in-focus images are obtained.

The contribution of this paper; although seems simple in its nature; is unique in that it alleviates most of the drawbacks of the CWAFT in data acquisition and processing. In addition, the pulse-echo nature of the PAFT, and the presence of many varieties of computer hardware such as array processors, accelerator cards and DSP chips makes it a good candidate for implementation in MI.

Images reconstructed using conventional pulse-echo techniques are based on projection and, thus, are convoluted by the measurement system response (transducers and propagation media). Thus, high-quality image reconstruction requires the use of wideband pulse-echo signals with higher dynamic range response. The proposed technique however, is based on the backward wave propagation (diffraction), uses a narrow pulse to focus the image and, therefore, remove the effect of the measurement response.

Throughout the formulation of the AFT algorithm, it was assumed; for simplicity, that the propagation medium has space attenuation only. Consideration for medical imaging and NDT should include frequency-dependent attenuation in the formulation. Comparisons should be made between the technique and conventional beam-former point-spread function.

REFERENCES

[1] A. Yamani and J. C. Bennett, 'Depth of field improvements and removal of distortion in long wavelength imaging systems," *Inst. Electr. Eng Proc.*, pt. F, vol. 132, no. 3, June 1985.

[2] J. W. Goodman, *Introduction to Fourier Optics*. New York: McGraw-Hill, 1968.

[3] L. J. Busse, "Three-dimensional imaging using a frequency-domain synthetic aperture focusing technique," *IEEE Trans. Ultrason., Ferroelec., Freq. Contr.*, vol. 39, no. 2, pp. 174–179, Mar. 1992.

[4] R. N. Bracewell, *The Fourier Transform and Its Applications*, 2nd ed. New York: McGraw-Hill, 1978.

[5] A. Yamani, "Three dimensional imaging using a new synthetic aperture focusing technique," *Int. Conf. Experimental Mechanic ICEM 96*, Singapore, Dec. 4–6 1996.

Limitations of the Principal-Axes Theory

Thorsten Schormann* and Karl Zilles

***Abstract*— The classical principal-axes transformation (PAT) has been used in numerous publications for three-dimensional (3-D) reconstructions by sequential alignment of histological sections. However, the PAT can determine at most $1/2n(n+1)$ parameters (scaling-rotation) in n dimensions. Distortions (shearing) of histological sections can be described by an affine transformation with n^2 parameters. An analytical model is devised for calculating rotational and scaling errors which can be determined by relating the transformation parameters of the PAT to the exact solution of a singular value decomposition (SVD) of the perturbation matrix. The results show that form and deformation of the form are intertwined and that these results can be transferred to real data. The model is important for assessing the quality that can be expected with the PAT for 3-D reconstructions if no multimodality reference is available (rigid transformation) and reveals the misalignment in terms of rotational and scaling errors resulting from the PAT as derived in a previously published paper [1].**

***Index Terms*— Affine transformation, principal-axes transformation, registration, 3-D reconstruction.**

I. INTRODUCTION

The difficulties encountered when registering a set of serial sections which are translated, rotated (and scaled) with respect to each other has been described in numerous publications using the well-known and well-established principal-axes transformation (PAT) [2], [3] whereby a three-dimensional (3-D) reconstruction is achieved by sequential alignment of consecutive sections, n sections apart [3]. The sections are treated as rigid bodies described by the inertia matrix from which the direction of the principal axes and moments of inertia can be calculated [7]. Due to lack of an appropriate multimodality reference, the PAT offers the possibility to reconstruct by superimposing the directions of the principal axes of consecutive sections. However, the PAT causes significant misalignment [3]. This misalignment has been attributed to the fact that sections that are far apart may not have overlapping principal axes [3]. In addition, small changes in the sizes and shapes of features were assumed in order to justify the applicability of the PAT. However, even in such cases significant misalignment can occur if the principal moments are about equal, that is, form and deformations of the form are intertwined. For example, the alignment of a minutely sheared square with a nondistorted square at the same position and the same orientation results in a rotational error of 45° when using the PAT, whereas the same shearing parameter applied to a rectangular shape, which is to be registered with an undistorted rectangle exhibits almost no rotational error.

A second important application of the PAT is the registration of two-dimensional (2-D) or 3-D objects resulting from the same

Manuscript received February 7, 1997. This study was supported by the Deutsche Forschungsgemeinschaft under Grant SFB 194/A6. The Associate Editor responsible for coordinating the review of this paper and recommending its publication was M. W. Vannier. *Asterisk indicates corresponding author.*

*T. Schormann is with the C. and O. Vogt Institute of Brain Research, Heinrich–Heine University Düsseldorf, Postfach 10 10 07, Düsseldorf D-40001 Germany (e-mail: thorsten@hirn.uni-duesseldorf.de).

K. Zilles is with the C. and O. Vogt Institute of Brain Research, Heinrich–Heine University Düsseldorf, Düsseldorf D-40001 Germany.

Publisher Item Identifier S 0278-0062(97)08956-8.